SSRG International Journal of Electrical and Electronics Engineering
ISSN: 2348-8379/ https://doi.org/10.14445/23488379/IJEEE-V13I11P114

Volume 13 Issue 11, 209-227, November 2026
© 2026 Seventh Sense Research Group®

Original Article

Super-Twisting Adaptive Robust Converter Control Framework for Grid-Connected PV-Battery EV Charging Systems

Jaganmohanrao Tarra[1], V Raja Kumar[2]

[1,2]*Department of Electrical, Electronics and Communication Engineering, GITAM Deemed to be University, Visakhapatnam, India.*
[1]*Department of Electrical and Electronics Engineering, Aditya Institute of Technology and Management, Tekkali, Andhra Pradesh, India.*

[1]*Corresponding Author: jaganmohan.tarra@gmail.com*

Received: 07 September 2026 Revised: 05 November 2026 Accepted: 18 November 2026 Published: 25 Novembr 2026

Abstract - *The rising use of renewable-integrated Electric Vehicle (EV) charging stations presents substantial dynamic issues at the grid interface and at DC-link stages, especially when fluctuating photovoltaic generation and changing EV loads. Although the use of Dynamic Voltage Restorers (DVRs) has become a standard practice to reduce external voltage disturbances at the point of common coupling, the overall system performance highly depends on the strength of internal converter control approaches. To improve the dynamic stability and power quality, this paper proposes Super-Twisting Adaptive Robust Converter (STARC) control strategy of grid-connected PV-battery-charging EV charging system. The STARC structure incorporates Robust Hybrid Reference Adaptation Control (RHRAC) for AC/DC grid-side converter to provide accurate current tracking, better power factor regulation and Hybrid Super-Twisting Cascaded PI Adaptive Control (HST-CPIAC) for the DC link that allows better DC-link voltage regulation, minimize ripple and provides a faster transient response. Extensive simulation in MATLAB/Simulink under fluctuating PV output and varying EV load scenarios demonstrates significant improvements over conventional PI-based control strategies. The STARC achieves a near-unity power factor of 0.998, reduced DC-link voltage ripple of 1.3%, fast dynamic response of 18 ms, settling time of 0.045 s, and a minimal tracking error of 0.7%, confirming its superiority and offers a high-performance internal control framework for next-generation grid-connected EV charging infrastructures.*

Keywords - *EV charging, STARC, Grid-Connected converters, RHRAC, DC-Link voltage control, HST-CPIAC, Power factor improvement.*

1. Introduction

EVs are growing rapidly along with renewable generation, which is changing the nature of the current power systems [1]. The technology that has received the most attention of all renewable technologies is from Photovoltaics (PV) because of their sustainable development capabilities and decreasing installation costs [2]. With the use of PV generation is integrated with battery energy storage in the EV charging infrastructure as one way of supporting cleaner transport, while additionally reducing grid dependency [3]. Both PV and battery installed in grid-connected EV charging systems are continually exposed to dynamic operating conditions because of solar energy's intermittent nature and variation with the stochastic behaviour of EV charging demand [4]. Because of this variability, there are several challenges related to the operation, stability, power quality, and reliable operation of these systems [5].

One of the main problems faced with these systems is how to properly regulate the DC-link voltage and run the grid-side converters during times of rapid changes in operating conditions [6]. For example, using solar energy that fluctuates as the sun shines or the use of electric vehicles that suddenly load can create a situation where the PCC could possibly experience problems due to instability of voltage and increased harmonics and poor power factor. Most of the grid disturbances are resolved using external compensation devices such as Dynamic Voltage Restorers (DVRs), but the overall performance of the system is primarily determined by how well the internal converter control strategies work [7]. Even though conventional Proportional-Integral (PI) controllers have become the most prevalent choice for use due to their relative ease of implementation and use, conventional PI controllers are typically at a disadvantage when compared to their counterparts because they do not have very good

This is an open access article under the CC BY-NC-ND license (http://creativecommons.org/licenses/by-nc-nd/4.0/)

robustness or do not respond quickly to dynamic operating changes, nor do they perform very well under conditions characterized by time-varying parameters and nonlinearities. To overcome these limitations, many researchers have been exploring advanced methods of Nonlinear Control Design Concepts [8]. The most popular control technique amongst them includes Sliding Mode Control (SMC), which is recognized around the world as having good robustness against disturbances [9]; however, SMC suffers from chattering, which can cause increased losses and decreased efficiency of the system. To mitigate these issues, higher-order sliding mode techniques such as Super Twisting Algorithm (STA) have been introduced [10, 11]. Integrating adaptive control mechanisms to enhance overall system performance has shown promising results [12]. The ability of adaptive forms of control to provide real-time adjustments to control parameters allows the system to respond more effectively through a wide range of parameter variations, nonlinearities, and external disturbances [13, 14].

Recent research has shown that the combination of adaptive control and higher-order sliding mode techniques has the potential to improve dynamic response, decrease steady-state error, and improve selected aspects of system performance [15]. However, many of these techniques either focus on grid-side converters or DC-link converters independently.

Also, some of them require intensive tuning, accurate model, or difficult computational optimization. Thus, there is a need for research in designing an integrated, adaptive and robust controller for converters. To meet this challenge, the proposed research suggests using a STARC control framework, where RHRAC can be used for controlling the grid-side converters and HST-CPIAC for DC-link voltage control.

The primary novelty of this research can be stated in the coordinated design of RHRAC and HST-CPIAC within the STARC framework. In contrast to the regular sliding mode and super twisting controllers that are used to control either grid-side current or DC-link voltage control, the proposed controller considers both. Moreover, the adaptation of reference values and gains provides better tracking and disturbance rejection.

The proposed approach is designed to reduce chattering, improve robustness, reduce ripple, and achieve fast dynamic response under varying PV generation and EV load conditions. The contribution of the paper is stated as,

- Proposes a novel STARC control framework to improve stability and power quality in grid-connected PV-battery EV charging systems.
- Develops RHRAC for accurate current tracking and enhanced power factor at the grid side.
- Introduces HST-CPIAC for efficient DC-link voltage regulation with reduced ripple and fast response.
- The coordination between RHRAC and HST-CPIAC is analyzed through MATLAB/Simulink, and the proposed method is compared with conventional control strategies.

The organization of the paper is as follows: Section 2 reviews the related work on grid-connected PV systems, EV charging infrastructures, and advanced converter control techniques. Section 3 presents the overall system configuration of the PV-battery EV charging system. Section 4 describes the proposed STARC control framework, including RHRAC and HST-CPIAC strategies. Section 5 discusses the simulation setup and performance results, and Section 6 concludes the paper and Section 7 discusses some limitations with future research directions.

2. Literature Review

This section reviews recent research on PV-battery EV charging systems and advanced converter control techniques. The review focuses on conventional PI control, Super-Twisting Sliding-Mode Control (STSMC), adaptive and intelligent control, and power-quality enhancement techniques. This highlights the limitations of existing methods and the need for more robust and adaptive control strategies.

2.1. Hybrid Energy Storage and EV Charging Architectures

The super-twisting synergetic sliding mode control scheme with adaptive barrier has been proposed by Zeb et al. [16] for smart electric vehicle charging stations. It includes the use of the hybrid energy storage system along with the MPPT scheme using RNNs for the PV panels and implements V2G, G2V, and V2V operations. The method provides enhanced robustness and energy efficiency along with stability but suffers from computational complexities and costly implementation. A methodology for managing the energy of a DC microgrid having hybrid renewable sources along with EVs has been suggested by Kumar et al. [17]. Batteries of EVs are used as buffers for regulating voltage variations, while the Bidirectional DC-DC Converter (BDDC) is supplemented with another voltage control loop. This approach enhances voltage stability and power balancing, but its complexity and converter synchronization are high, and only a particular experimental setup has been tested with this approach.

2.2. DC-Bus Voltage Regulation and Power Sharing

A robust Integral Super-Twisting Algorithm (ISTA) controller with adaptive gain for a PV-integrated hybrid energy storage system was proposed by Benadli et al. [18]. A regulator regulates the DC bus voltage and current. The main advantages of ISTA over PI controller include reduced rise time, zero percent overshoot, zero steady state error, and effective power distribution between storage units. Because of its nonlinear design, it is hard to implement.

Wahidi et al. [19] suggested the use of adaptive droop control in DC microgrid systems that are isolated, consisting of solar energy sources, wind energy sources, fuel cells, batteries, and electric vehicles as flexible energy sources. Adaptive droop values provide stable DC-bus voltages and proper power sharing with changing renewable sources. Conventional PI and fixed droop control approaches do not have such capability for adaptive regulation of the voltage.

Anbuchandran et al. [20] have used the STSMC strategy to regulate voltage dynamically in DC microgrid systems with solar, wind, hydrogen, and battery as sources. The multiport DC-DC converter takes care of the variations in both supply and demand. This technique enhances stability and response time during transients. It is limited by additional complexity in control and implementation.

2.3. Sliding-Mode and Super-Twisting Control

The main reason for the popularity of sliding mode control in converters is due to its robustness toward disturbances and parameter uncertainties. However, its principal disadvantage is chatter. The super-twisting (second-order sliding mode) technique helps decrease chatter while preserving the robustness feature, and some of the papers [16, 18, 23] use it. Mondal et al. [21] evaluated the coordination of grid-connected hybrid renewable energy system by utilizing the STSMC strategy. Chatter can be suppressed by this algorithm, which helps deal with the power fluctuation problem, allows stable performance under generator and load conditions, increases voltage stability, decreases harmonics and handles the reactive power problem.

2.4. Intelligent and Optimisation-based Control

The researchers Zeeshan and Srivastava, [22] investigated the effect of EV charging on grid-connected hybrid wind and solar PV generation systems using ANFIS for enhancement in power quality. The study conducted an analysis of battery and supercapacitor sizing and concluded that the PI controller results in unbalance in currents and harmonic distortion during EV charging process. The gains of a grid-connected solar inverter, namely, the Kp, Ki, and Kd of the PID controller, were optimized by Gupta et al. [23] through GWO. This approach has been formulated based on the minimization of mean square error and THD. Hence, the voltage regulation is stable with low THD value compared to other PI/P regulators. This process increases the computational complexity and requires optimisation.

2.5. Power-Quality and Grid-Interface Control

An adaptive tracking control has been suggested by Mishra et al. [24] for multi-source bidirectional EV charging. The error-based technique is equipped with frequency estimation and multi-resonant direct power control, which provides precise tracking, harmonic reduction, DC offset elimination and switching noise removal, as well as unity power factor. This technique complicates the control system and requires real-time signal processing. The eMSOGI-based UPQC control strategy for EV chargers is proposed by Kumar et al. [25]. Using cascaded adaptive notch filters, the fundamental component is isolated. This helps to reduce the THD and enhance the signal synchronization. The disadvantages are increased complexity of the control algorithm and high sensitivity of the notch filter tuning. Table 1 summarizes the reviewed literature.

Table 1. Summary of reviewed literatures

Ref.	Approach	System	Main strength	Main limitation
[16]	Adaptive barrier super-twisting synergetic SMC + RNN-MPPT + GA	EV station, HESS, V2G/G2V/V2V	Stability, robustness, efficiency	Computational complexity, cost
[17]	BDDC with extra voltage loop	DC microgrid, EVs	Voltage regulation, power balance	Converter coordination, complexity
[18]	Adaptive-gain ISTA	PV-HESS DC microgrid	Zero overshoot, fast response	Nonlinear design complexity
[19]	Adaptive droop	Islanded DC microgrid	Accurate power sharing	Parameter tuning
[20]	ANFIS	Grid-connected wind-PV with EVs	Lower THD, balanced voltage/current	Needs models and training
[21]	Super-twisting SMC	Grid-connected hybrid renewable	Stability, reduced harmonics	Hardware and implementation difficulty
[22]	GWO-tuned PID	Grid-connected solar inverter	Lower THD, better transient	Optimisation overhead
[23]	STSMC with multiport converter	Hybrid DC microgrid	Fast transient response	Real-time implementation
[24]	Multi-resonant direct power control	Bidirectional EV charger	Harmonic and DC-offset reduction	Real-time processing needs
[25]	eMSOGI-UPQC	EV charging station	Harmonic suppression	Notch-filter tuning

2.6. Research Gap Identification

Although there have been many advancements in control strategies for controlling grid-connected systems, many research gaps remain.

Limited robustness of tuned and intelligent controllers: Traditional PI controllers and optimised GWO-PID [22]/ANFIS [20] controllers help improve steady-state operating performance, but they do not show any robustness to sudden fluctuations in PV power output and/or rapidly changing EV loads.

Trade-offs in Droop and adaptive control methods: This helps to provide power-sharing amongst multiple inverters connected to a grid and manage the interaction with the grid, but there is generally a trade-off between voltage stability, transient response and tracking accuracy.

Converter chain applicability: Super-twisting and sliding mode controllers increase robustness; however, they are typically studied with either grid-side or DC-link control methods [16, 18]; very few studies attempt to develop a complete, integrated control system. Computationally Expensive: In addition, many of these control methods rely on precise tuning of parameters and/or extensive computational modelling or optimization, which hinders their ability to operate in real-time. Many solutions such as DVRs are used to reduce external disturbances and improve power quality. However, less focus has been given to improving internal converter control for overall system stability. Therefore, it may be possible to develop a unified adaptive and robust control framework that could provide simultaneous improvement of power quality and DC-link voltage regulation. This is the motivation behind the development of the proposed STARC approach.

3. Proposed System

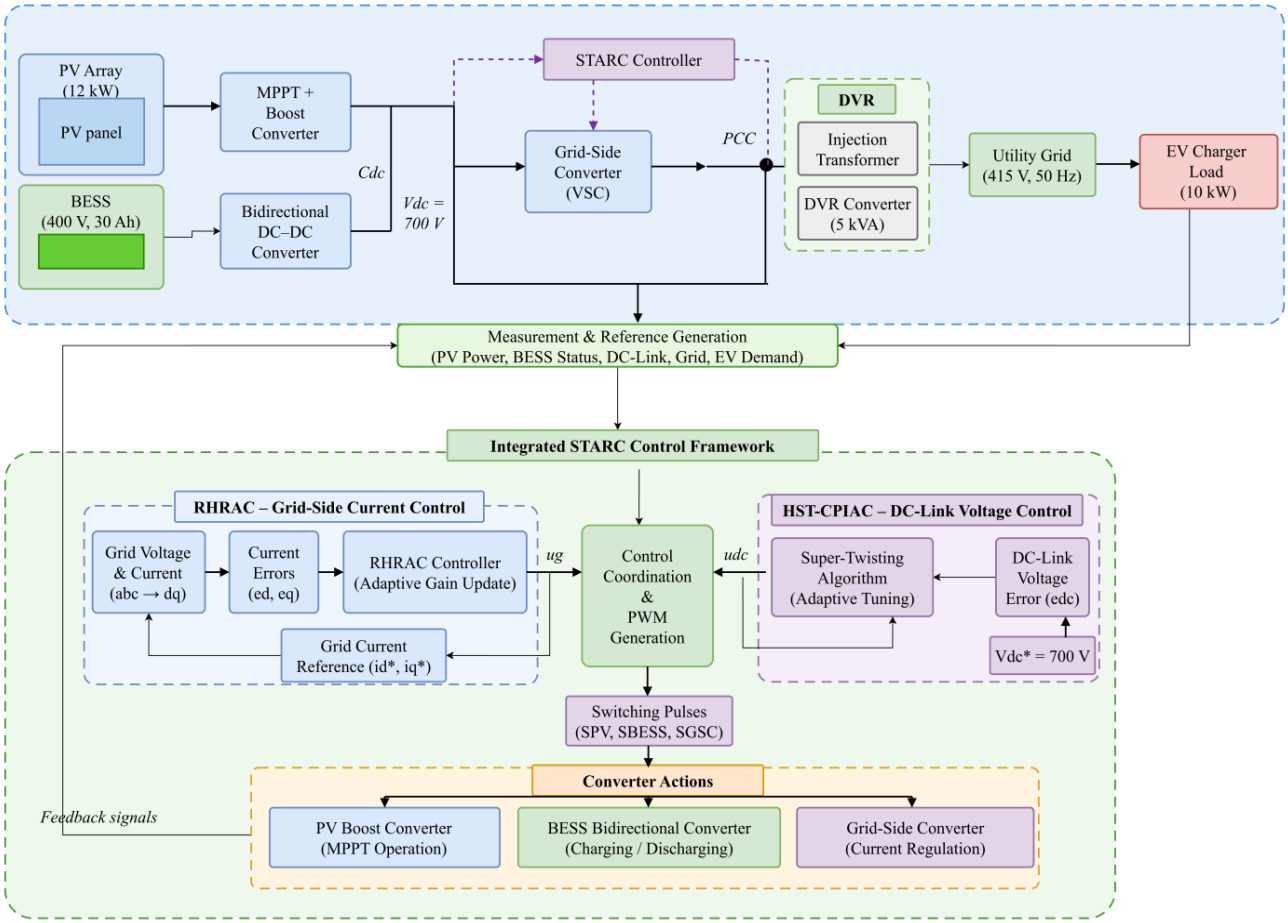

Fig. 1 Block diagram of proposed control framework

The proposed methodology includes a grid-connected photovoltaic/battery-powered electric vehicle charging system coordinated through a DC-link and controlled by the STARC framework. The photovoltaic array operates under an MPPT control to obtain maximum power from the array, which is controlled by a DC-DC converter and supplied to the DC-link. The battery is also connected to provide energy balancing during fluctuations.

The three-phase Voltage Source Converter (VSC) serves as the interface between the DC link and the AC supply, whereas the Dynamic Voltage Restorer (DVR) is coupled to

the system through common coupling point using a series injection transformer to regulate voltage sags and reduce grid-side disturbances.

The AC/DC converter connects the grid to the DC-link to provide bidirectional power flow. The RHRAC controller provides accurate grid-side current tracking and unity power factor, while the HST-CPIAC controller provides DC-link voltage stability for robust and efficient performance.

The proposed control framework's block diagram is shown in Figure 1.

3.1. System Configuration and Mathematical Modelling

The proposed system comprises a grid-connected hybrid power system, which includes a PV system, a BESS, an EV charging load, and a bidirectional grid interface. The STARC framework uses RHRAC for grid-side current control and HST-CPIAC for DC-link voltage control. The circuit-level configuration of the proposed PV-BESS integrated grid-connected EV charging system is depicted in Figure 2(a). A DC-link is commonly used as a connection point for all power components. This enables power sharing between all components. The Dynamic Voltage Restorer (DVR) system is presented in Figure 2(b), which is integrated in series between the grid and common coupling point of the charging system. It works by using compensating voltage through a series filter to lessen grid-voltage disturbances and maintain load-voltage stability.

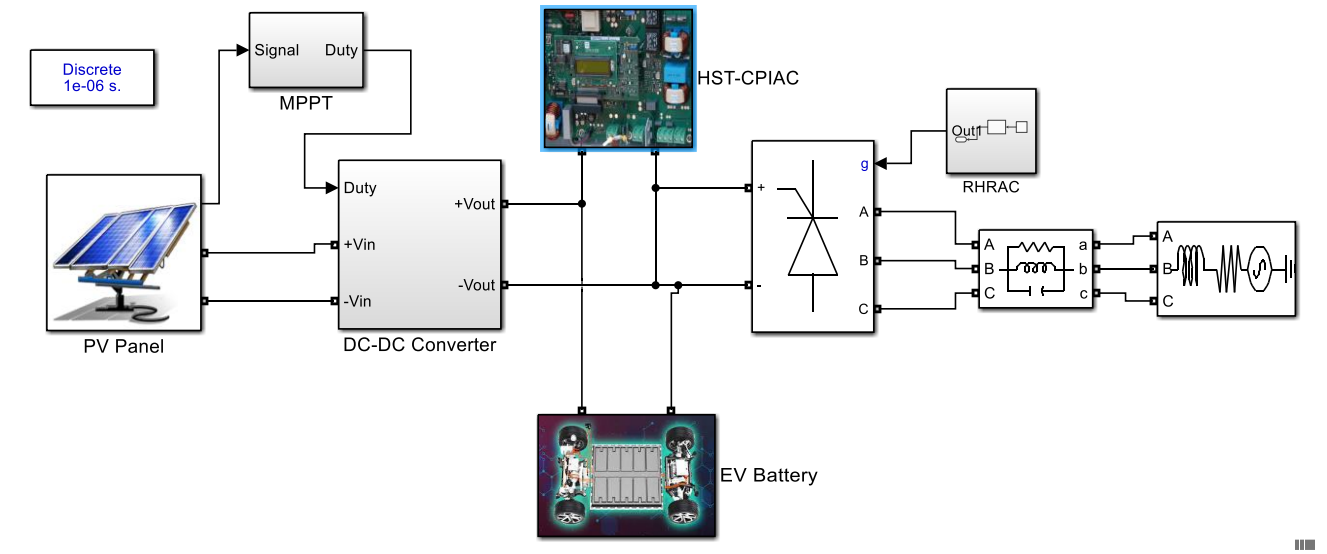

(a)

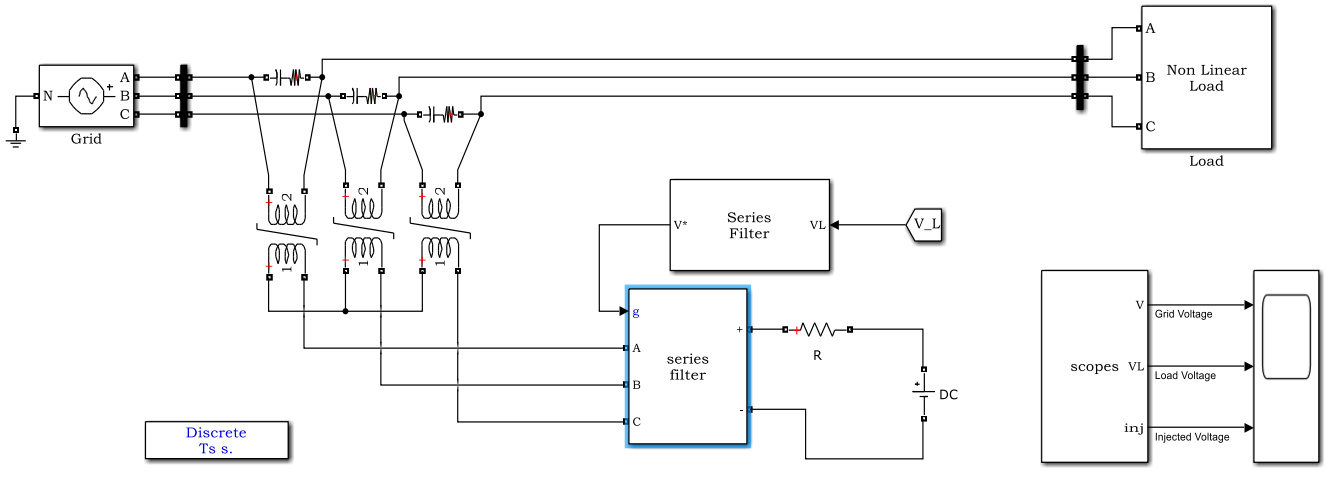

(b)

Fig. 2 Circuit-Level configuration (a) Proposed grid-connected PV-Battery EV charging system, and (b) DVR configuration.

The PV system acts as the primary source of renewable energy, and the battery acts as the source of energy buffering to account for the intermittency and sudden changes in the loads. The grid interface maintains the stability of the system by injecting or absorbing power during deficit and surplus periods. The EV charge load connections are made to the DC link for efficient charging. The power balance of the system is maintained by:

$$P_{PV} + P_{bat} + P_{grid} = P_{EV} + P_{loss} \quad (1)$$

Where P_{PV}, P_{bat}, and P_{grid} denote the power contributions from the PV array, battery, and grid, respectively, while P_{EV} represents the EV load demand and P_{loss} accounts for system losses. Table 2 describes the proposed system design parameters.

Table 2. System design parameters

Component	Typical Rating
EV Battery Pack	400 V, 25 Ah - 50 Ah (10 kWh - 20 kWh)
EV Charger Power	10 kW
PV Array	12 kW (oversized)
PV Voltage	600 - 700 V DC
Battery Energy Storage (BESS)	400 V, 30 Ah (≈12 kWh)
DC Link Voltage	700 V
Grid Voltage	415 V L-L, 50 Hz
Grid Side Converter (VSC)	15 kVA
DC-DC Converter (PV Boost)	12 kW
Battery Bidirectional Converter	10 kW
DVR Rating	5 kVA
DVR Injection Transformer	415/150 V
Filter Inductor (L)	3-5 mH
DC Link Capacitor	2200 - 4700 µF

3.1.1. Photovoltaic System Modeling

The PV system can be represented by an equivalent circuit based on a well-established single-diode model. This model can accurately characterize the non-linear behaviour of the current and voltage of a solar cell under different environmental conditions. This model considers the series resistance, shunt resistance, and diodes. The PV output current can be expressed as:

$$I_{PV} = I_{ph} - I_0\left(e^{\frac{V_{PV}+I_{PV}R_S}{nV_t}} - 1\right) - \frac{V_{PV}+I_{PV}R_S}{R_{sh}} \quad (2)$$

Where I_{ph} is the photo-current, I_0 is the saturation current in the diode, R_s and R_{sh} represent the series and shunt resistances respectively, while V_t denotes the thermal voltage. The power generated by the PV system is expressed as:

$$P_{PV} = V_{PV} \cdot I_{PV} \quad (3)$$

To maximize power extraction from the solar source, the Maximum Power Point Tracking (MPPT) technique is used. For this purpose, the operating condition is

$$\frac{dP}{dV} = 0 \Rightarrow \frac{dI}{dV} = -\frac{I}{V} \quad (4)$$

3.1.2. Battery Energy Storage System (BESS) Modeling

The BESS is modeled to account for its dynamic behavior in terms of the charging and discharging operations. State of Charge (SOC) is considered a significant parameter to measure the available energy in the battery. It varies according to the change in the current over time. The SOC can be represented as:

$$SOC(t) = SOC(t_0) + \frac{1}{C_{bat}}\int_{t_0}^{t} I_{bat}\,(t)\,dt \quad (5)$$

Where C_{bat} represents the battery capacity and I_{bat} denotes the battery current. The battery terminal voltage is modeled as:

$$V_{bat} = V_{oc}(SOC) - R_{int}I_{bat} \quad (6)$$

Where V_{oc} signifies the open-circuit voltage and R_{int} denotes the internal resistance. To ensure safe and reliable operation, the SOC is constrained within permissible limits:

$$SOC_{min} \leq SOC \leq SOC_{max} \quad (7)$$

3.1.3. Power Converter Modeling

A reference frame that rotates at the same frequency as the electric grid represents the grid-side converter dq This decouples the control of active and reactive parts of the power. Decoupling the control of currents improves the performance of the system. The dynamic equations for the converter's current can be represented as:

$$L\frac{di_d}{dt} = -Ri_d + \omega Li_q + V_d - V_{gd} \quad (8)$$

$$L\frac{di_q}{dt} = -Ri_q - \omega Li_d + V_q - V_{gq} \quad (9)$$

Where $i_d$and i_q terms indicates the direct and quadrature axis current,V_d and V_q signifies the converter voltages, and V_{gd}, V_{gq} signifies the grid voltages in the dq-frame. The DC-link capacitor plays a crucial role in maintaining voltage stability and is modelled as:

$$C_{dc}\frac{dV_{dc}}{dt} = I_{in} - I_{out} \quad (10)$$

or equivalently in power form:

$$C_{dc}V_{dc}\frac{dV_{dc}}{dt} = P_{in} - P_{out} \quad (11)$$

3.2. Proposed STARC Framework

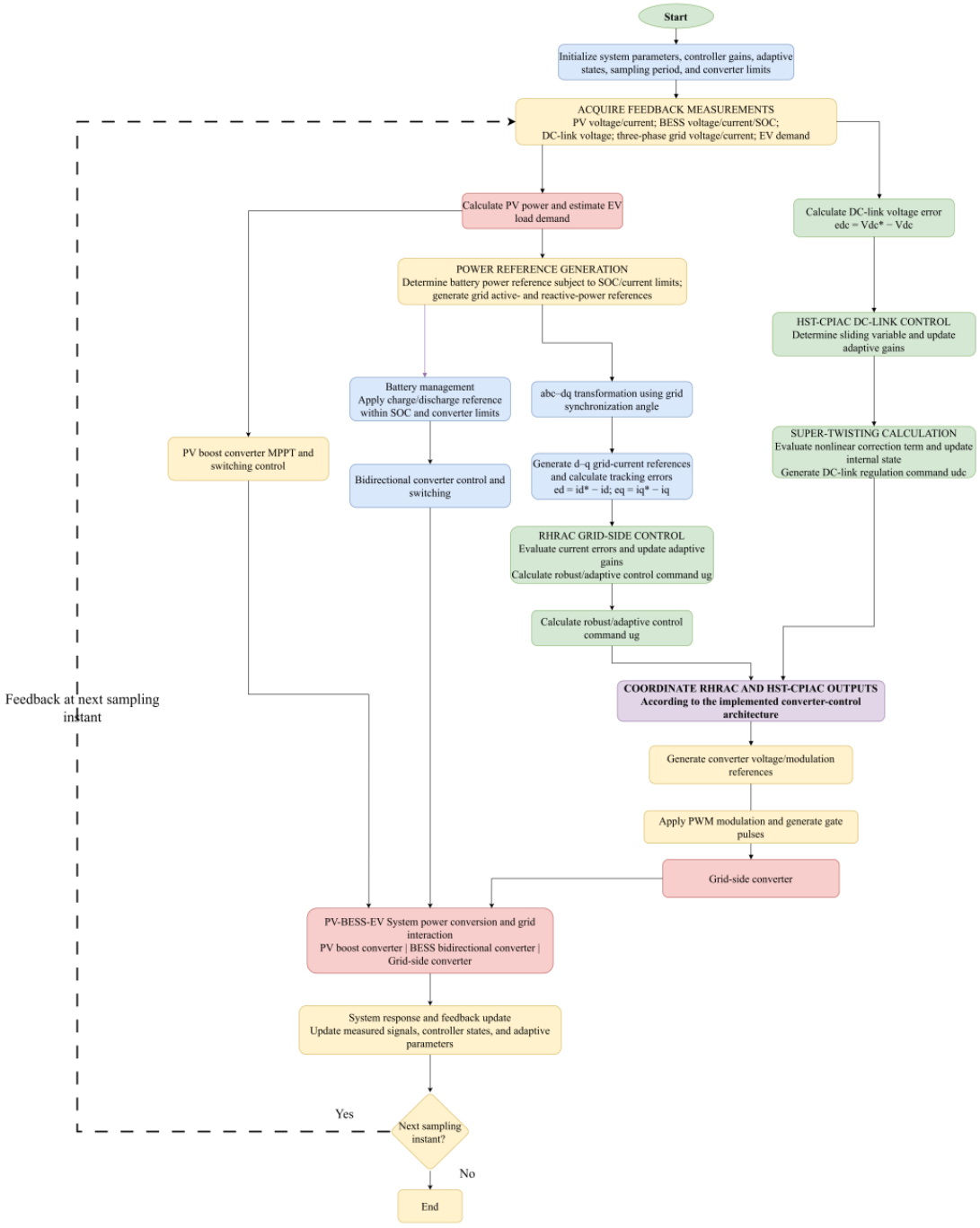

Fig. 3 Systematic flowchart of control framework

The control structure STARC has been introduced to provide robustness to the system and to enhance the dynamic performance of the system. This type of control mechanism combines super twisting sliding mode control with adaptive control to minimize chattering and achieve faster convergence. Two control structures have been proposed in STARC. In the first control structure, the grid-side controller has been implemented using the Robust Hybrid Reference Adaptive Control (RHRAC) to control the current and improve the power factor.

In the second control structure, the DC-link controller has been implemented using the Hybrid Super-Twisting Cascaded PI Adaptive Control (HST-CPIAC), which controls the DC-link voltage. The flowchart of this control structure is represented in Figure 3. To check the stability of the proposed controller, Lyapunov stability analysis has been conducted by calculating the tracking error. In general, the tracking error has been represented as:

$$e = x - x^* \tag{12}$$

Where x is the system state and x^* is the reference value.

3.2.1. Grid-Side Control using RHRAC

The primary responsibility of the grid-side controller is to maintain the accuracy of the current tracking while keeping the power factor at unity.

The RHRAC strategy regulates the reference currents and uses super twisting control for robustness against disturbances and uncertainties. The current tracking error is defined as:

$$e_d = i_d - i_d^*,\ e_q = i_q - i_q^* \tag{13}$$

The corresponding sliding surfaces are:

$$s_d = e_d,\ s_q = e_q \tag{14}$$

The control law for super-twisting is expressed as in the form of internal state variables (x_1, x_2).

$$u_d = -k_1|s_d|^{1/2}\text{sign}(s_d) - k_2\int \text{sign}(s_d)\,dt \tag{15}$$

$$u_q = -k_1|s_q|^{1/2}\text{sign}(s_q) - k_2\int \text{sign}(s_q)\,dt \tag{16}$$

$$x_1 = -k_1|s|^{1/2}\text{sign}(s) \tag{17}$$

$$x_2 = -k_2\int \text{sign}(s)\,dt \tag{18}$$

The reference currents are generated as:

$$i_d^* = \frac{2P^*}{3V_d},\ i_q^* = 0 \tag{19}$$

To enhance adaptability, the reference current is updated as:

$$i_d^* = i_d^* + \alpha e_d \tag{20}$$

The input control signal given to the converter is described by:

$$V_d = L\frac{di_d}{dt} + Ri_d - \omega Li_q + u_d \tag{21}$$

$$V_q = L\frac{di_q}{dt} + Ri_q + \omega Li_d + u_q \tag{22}$$

3.2.2 DC-Link Control using HST-CPIAC

The DC-link controller is designed to control DC voltage in varying conditions such as fluctuations in PV and disturbances in EV loads. HST-CPIAC is a control strategy that utilizes the benefits of both STC and Adaptive PI to obtain fast response and zero error in steady states.

The voltage tracking error is defined as:

$$e_v = V_{dc} - V_{dc}^* \tag{23}$$

The sliding surface is given by:

$$s_v = e_v \tag{24}$$

The super-twisting control input is expressed as:

$$u_v = -k_1|s_v|^{1/2}\text{sign}(s_v) - k_2\int \text{sign}(s_v)\,dt \tag{25}$$

The PI controller generates the reference current as:

$$i_d^* = K_p e_v + K_i\int e_v\,dt \tag{26}$$

To improve adaptability, the controller gains are updated dynamically:

$$K_p = K_{p0} + \gamma_1|e_v|,\ K_i = K_{i0} + \gamma_2|e_v| \tag{27}$$

The final hybrid control law is expressed as:

$$i_d^* = \left(K_p e_v + K_i\int e_v\,dt\right) + u_v \tag{28}$$

DVR controls the load side voltage by applying the series compensation voltage. The value of compensation voltage is by the difference between desired load voltage and measured grid voltage. This unified STARC framework enables coordination between the grid-side converter control and the DC-link dynamics. This integrated approach enables the simultaneous control of the currents and voltages in the system, thereby ensuring stability under nonlinear and uncertain conditions.

4. Result Analysis

The suggested grid-connected PV-battery EV charging system with the STARC control method is executed in MATLAB-Simulink to test the performance of the system under both dynamic and steady-state operating conditions. For testing purposes, various operating scenarios are considered to check the robustness and flexibility of the suggested control method. For instance, various levels of solar irradiance, sudden changes in the EV load, and grid voltage are considered to test the performance of the suggested grid-connected PV-battery EV charging system. Various key parameters, such as voltage stabilization, grid current, grid voltage, and power factor, are continuously monitored to test the performance of the suggested system.

4.1. Simulation Setup and Parameters

The implementation of the proposed STARC in MATLAB/Simulink is depicted in Figure 4, where error calculations, reference generation, and a control block based on a super-twisting algorithm with a sliding mode control are included to guarantee performance in tracking control. A sliding manifold is designed based on error dynamics, and an integral algorithm is utilized to reduce chattering and improve convergence rate, with disturbance signals added to test system robustness.

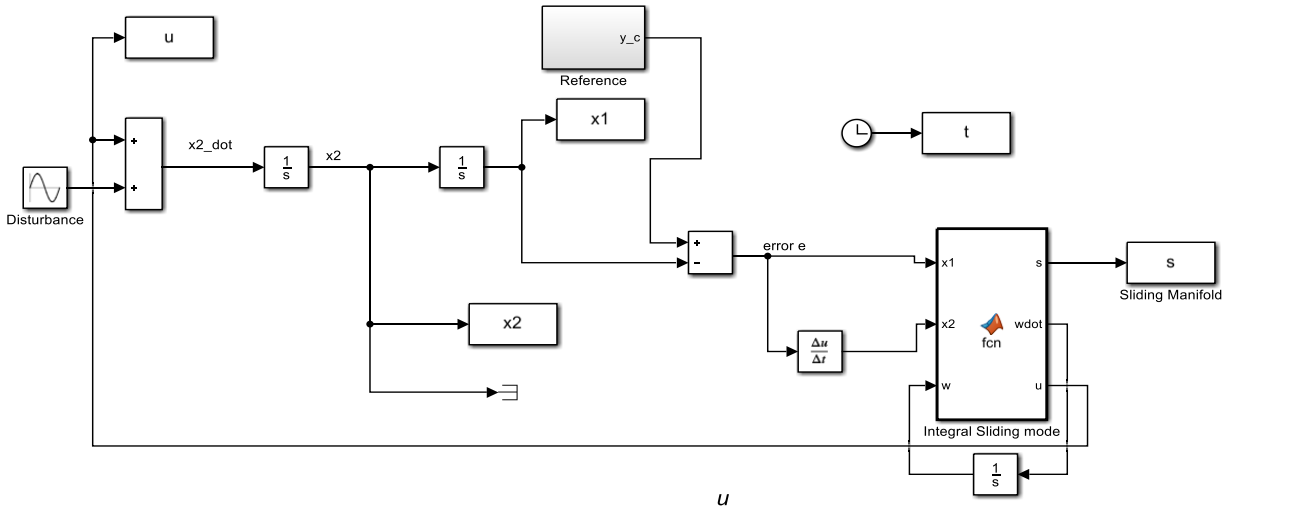

Fig. 4 Simulink implementation of super-twisting adaptive robust controller

The entire implementation shows that the controller can handle non-linearities and parameter variations, providing a stable control action. Parameters used in STARC are explained in Table 3 along with parameter settings adopted for each controller. Table 4 gives the values for each simulation parameter.

Table 3. Parameter description of STARC

Parameter	Symbol	Description	Function in Controller
Grid d-axis current	i_d	Actual d-axis current	Used for active power control
Grid q-axis current	i_q	Actual q-axis current	Used for reactive power control
Reference d-axis current	i_d^*	Desired d-axis current	Ensures active power tracking
Reference q-axis current	i_q^*	Desired q-axis current (zero)	Maintains unity power factor
Current errors	e_d, e_q	Difference between actual and reference currents	Drives grid-side controller
Voltage error	e_v	Difference between DC voltage and reference	Drives DC-link controller
Sliding surfaces	s_d, s_q, s_v	Defined from respective errors	Represents system deviation
Super-twisting gain 1	k_1	Nonlinear gain	Controls convergence speed
Super-twisting gain 2	k_2	Integral gain	Ensures finite-time convergence

Internal state 1	x_1	Nonlinear control term	$-k_1\|s\|^{1/2}\text{sign}(s)$
Internal state 2	x_2	Integral control term	$-k_2\int \text{sign}(s)\,dt$
Super-twisting control inputs	u_d, u_q	Control signals for dq axes	Enhance robustness and tracking
DC-link control input	u_v	Super-twisting voltage control signal	Stabilizes DC-link voltage
Active power reference	P^*	Desired power	Used to compute i_d^*
Grid voltage (d-axis)	V_d	Grid voltage in dq frame	Used in current reference generation
Adaptation gain	α	Error-based tuning parameter	Improves reference tracking
PI proportional gain	K_p	Proportional gain	Reduces instantaneous error
PI integral gain	K_i	Integral gain	Eliminates steady-state error
Adaptive gains	γ_1, γ_2	Gain tuning coefficients	Adjust K_p, K_i dynamically
Inductance	L	Filter inductance	Affects current dynamics
Resistance	R	Filter resistance	Represents system losses
Angular frequency	ω	Grid angular frequency	Enables d, q transformation
DC-link voltage	V_{dc}	Actual DC voltage	Controlled variable
Reference DC voltage	V_{dc}^*	Desired DC voltage	Stability target
Converter voltages	V_d, V_q	Control inputs to converter	Regulate current flow

Parameter settings adopted for each controller

Controller	Parameter 1	Parameter 2	Parameter 3	Tuning objective
Fuzzy MPPT	Membership functions: 7	Input scaling factor: 0.85	Output scaling factor: 0.12	Minimize tracking error and oscillations
HC	Perturbation step size: 0.002	Sampling time: 0.01 s	Step adjustment factor: 0.5	Balance convergence speed and oscillations
INC	Conductance increment: 0.001	Sampling time: 0.01 s	Step adjustment factor: 0.5	Improve tracking accuracy and convergence
P&O	Perturbation step size: 0.0015	Sampling time: 0.01 s	Adaptive factor: 0.4	Minimize steady-state oscillations
Proposed	Controller gain \(K_p\): 1.5	Controller gain \(K_i\): 0.8	Optimization factor: 0.95	Minimize overall tracking error and settling time

Table 4. Simulation parameters and values

Parameter	Value	Unit
PV rated power	10	kW
PV nominal voltage	300	V
DC-link voltage	700	V
Grid phase voltage	240	V
Grid line voltage	415	V
Grid frequency	50	Hz
Boost converter inductance	3	mH
Input capacitance	2200	µF
DC-link capacitance	4700	µF
Input resistance	0.1	Ω
Boost converter switching frequency	10	kHz
Nominal duty cycle	0.571	-
Grid filter inductance	2	mH
Grid filter resistance	0.1	Ω
Inverter switching frequency	10	kHz

DC-link voltage PI gain	0.5	-
DC-link voltage integral gain	50	-
Grid current PI gain	2	-
Grid current integral gain	100	-
Battery current PI gain	0.2	-
Battery current integral gain	20	-
Battery nominal voltage	400	V
Battery capacity	100	Ah
Initial battery SOC	60	%
Maximum battery charging power	6	kW
Maximum battery discharging power	6	kW
MPPT sampling time	1	ms
Controller sampling time	100	µs
Powergui sample time	2	µs
Visible values		
Parameter	Visible value	Unit
Solar irradiance	1000	W/m²
PV temperature	25	°C
powergui sample time	3×10^{-5}	s

4.2. Performance Measures

Power Factor: Represents synchronization between voltage and current waveforms. A value near one, PF allows for optimal transmission of power.

$$PF = \cos(\phi) = \frac{P}{\sqrt{P^2+Q^2}} \tag{29}$$

Voltage Stabilization (%): Evaluates the difference between output voltage and its reference; smaller difference gives better regulation.

$$\%V_{stab} = \frac{|V_{dc}-V_{dc}^*|}{V_{dc}^*} \times 100 \tag{30}$$

Ripple (%): It measures DC-link voltage variation around its mean value; low ripple will make the system operate smoothly.

$$\%Ripple = \frac{V_{max}-V_{min}}{V_{avg}} \times 100 \tag{31}$$

Dynamic Response (ms): Time required for the system to react to a perturbation or variation in the input (rise time).

$$t_r = t_{90\%} - t_{10\%} \tag{32}$$

Settling Time (s): Time required for the response to stay within a tolerance band (typically ±2% or ±5%).

$$t_s = \text{time when } \left|y(t) - y_{ss}\right| \leq \epsilon \tag{33}$$

Tracking Error (%): Difference between reference and actual value; lower error indicates accurate control.

$$\%e = \frac{|x-x^*|}{x^*} \times 100 \tag{34}$$

Table 5. Dynamic simulation operating conditions

Condition	Irradiance (W/m²)	EV load (kW)	Battery charging (kW)	Battery discharging (kW)	Grid voltage (V)
1	200	2	1	0	180
2	400	4	2	0	190
3	600	6	3	0	200
4	800	8	0	4	210
5	900	10	0	5	220
6	1000	12	0	6	230

Operating conditions considered in the dynamic analysis of the proposed STARC control strategy are shown in Table 5. In this case, there are six operational scenarios with variations of PV irradiation, EV charging demands, battery charging/discharging power, and grid voltage. The analysis of the response of the system under different conditions of power generation, EV load, battery operation and grid voltage is analyzed quantitatively in Table 6. In this analysis, power balance is done by considering PV power generation, battery charging/discharging, EV demand, and converter losses.

Table 6. Quantitative power flow analysis

Condition	Irradiance (W/m²)	PV (kW)	EV (kW)	BESS charge (kW)	BESS discharge (kW)	Grid import (+) / export (−) (kW)	Losses (kW)
1	200	2	2	0	0	0.06	0.06
2	400	4	3	0.8	0	−0.11	0.09
3	600	6	6	0	0	0.18	0.18
4	800	8	6	1.5	0	−0.32	0.18
5	900	9	10	0	1	0.3	0.3
6	1000	10	10	0	1.5	-1.14	0.36

Figure 5 shows the current and terminal voltage of EV with the proposed STARC control strategy. As can be seen from Figure 5, the charging current of the EV demonstrates smooth and quick transient behavior to attain its steady-state value without much overshoot. At the same time, the terminal voltage of EV battery remains constant with low ripple and quick transient behavior, demonstrating stable response of the proposed control strategy.

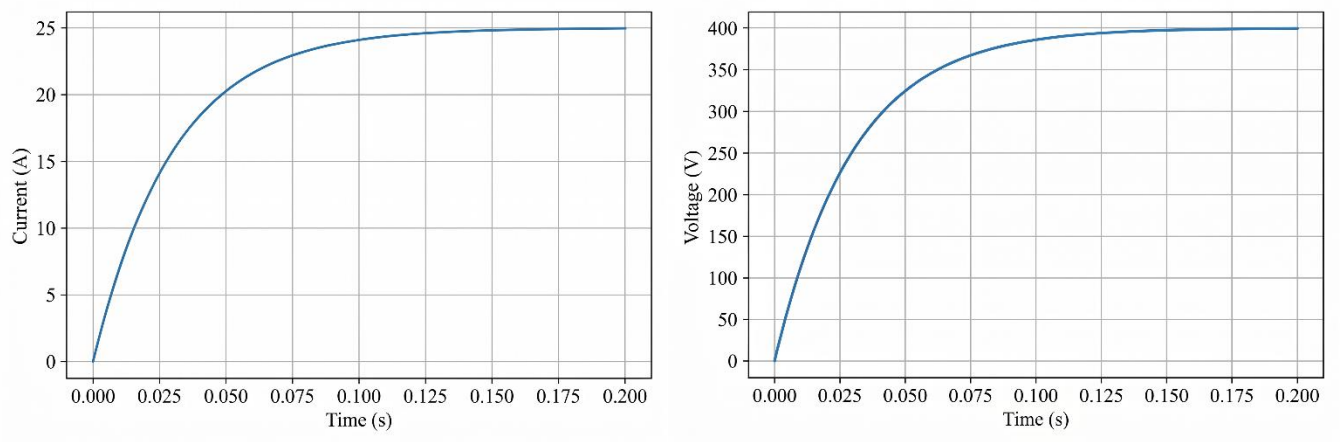

Fig. 5 Analysis of EV current and voltage

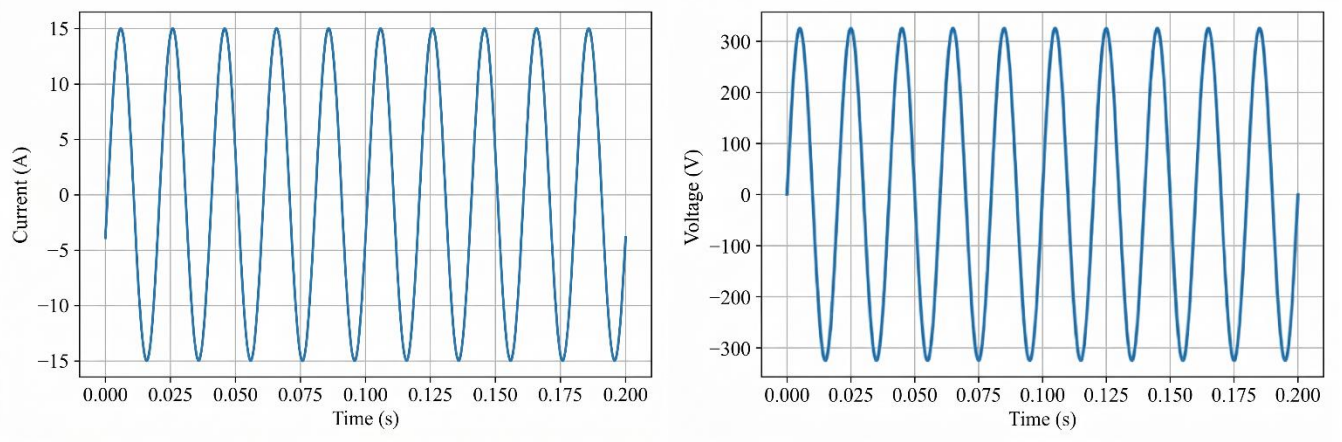

Fig. 6 Analysis of grid current and voltage

Figure 6 shows the current waveform at the grid side when the STARC method is employed. The current shows a clean sinusoidal shape with minimal distortion, indicating that the current is well regulated and that harmonic suppression is effective. The magnitude is constant, showing that the current is well regulated and that power exchange with the grid is effective. Furthermore, the current is in phase with the voltage, showing that the power factor is close to unity. The absence of oscillations in the current shows that the control method is robust.

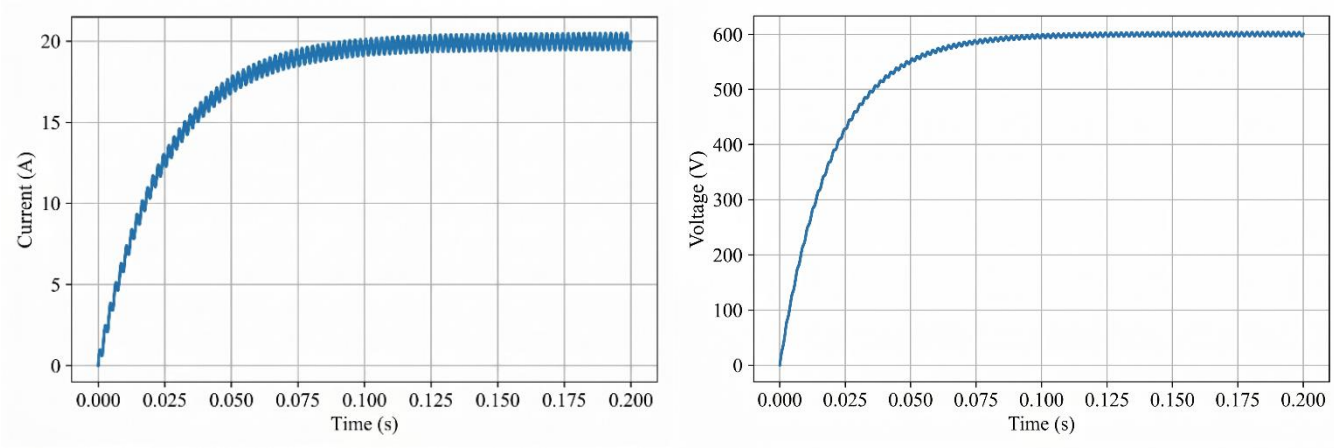

Fig. 7 Analysis of PV current and voltage

Figure 7 shows the dynamic response of the photovoltaic current and voltage under the suggested STARC-controlled system. As shown, the current drawn from the PV system smoothly increases and reaches its steady-state value without any oscillations, verifying the effective MPPT performance. At the same time, the voltage response of the PV system rapidly reaches its optimum operating point with minimal dynamic disturbances. The absence of overshoot and the steady-state response verify the stability performance under varying irradiances. Therefore, the suggested control framework is efficient in extracting the maximum power from the PV system with stable voltage and minimal dynamic disturbances.

Table 7. Comparative analysis of control strategies

Method	Power Factor	Voltage Stabilization (%)	Ripple (%)	Dynamic Response (ms)	Settling Time (s)	Tracking Error (%)
Conventional PI Control [14]	0.93	4.8	5.2	55	0.12	4.5
Sliding Mode Control (SMC) [21]	0.96	3.5	3.8	40	0.09	3.2
Adaptive Control [24]	0.97	2.9	3.1	32	0.07	2.4
mSOGI-based Control [25]	0.98	2.2	2.6	26	0.06	1.8
Proposed STARC (RHRAC-HST-CPIAC)	0.9993	1.1	1.3	18	0.045	0.7

Table 7 compares different control techniques and shows the superiority of the developed STARC technique. The performance of a conventional PI controller is poor, as shown by a 5.2% ripple, a slow response, and a power factor of 0.93. Sliding Mode Control provides robust control but results in a moderate ripple. Adaptive control provides better stability along with a reduced error. In addition, a power factor of 0.98, a reduced ripple of 2.6%, a faster response time of 0.06 s, and a reduced error are obtained by the mSOGI technique, indicates better synchronization and lower distortion. However, the developed STARC technique provides a power factor of 0.9993, a minimum ripple of 1.3%, a fast response time of 18 ms, a minimum settling time of 0.045 s, and a minimum error of 0.7%, ensuring robust and efficient operation.

4.3. Power Quality Analysis

Power quality analysis will help to check whether the design of the controller ensures stability of the voltage and current, decreases harmonics, reactive power control, and improvement of the power factor during grid-connected operation.

Table 8. Power-Quality parameters

Parameter	Values	Unit
Grid line voltage	415	V
Grid phase voltage	240	V
Grid frequency	50	Hz
Rated inverter power	15	kW
Fundamental grid current	20.87	A
Active power	15	kW
Reactive power	0.45	kVAr
Apparent power	15.007	kVA
Power factor	0.9995	-
Grid-current THD	2.1	%

Grid-voltage THD	1.2	%
Fundamental displacement factor	0.9995	-
Peak current	29.51	A
RMS current	20.87	A

Table 8 shows the value of power quality parameters for the proposed controller. Table 9 compares the conventional controller with proposed STARC controller based on grid-side power quality parameters.

The results show that the proposed STARC controller outperforms the conventional controller with respect to harmonic reduction, reactive power exchange and power quality index improvement.

Table 9. Comparative power-quality analysis

Power-quality parameter	Conventional control	Proposed control	Unit
Grid-current THD	8.5	2.1	%
Grid-voltage THD	3.2	1.2	%
Reactive power	4.5	0.45	kVAr
Displacement power factor	0.958	0.9995	-
True power factor	0.955	0.9993	-
Grid RMS current	21.78	20.87	A
Active power	15	15	kW
Apparent power	15.66	15.007	kVA

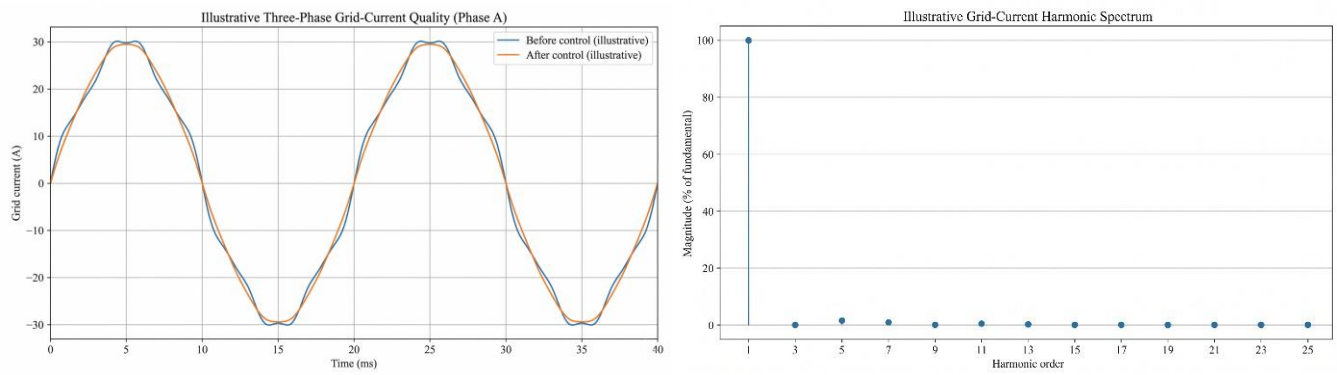

Fig. 8 (a) Grid current response, and (b) Harmonic spectrum of the grid current.

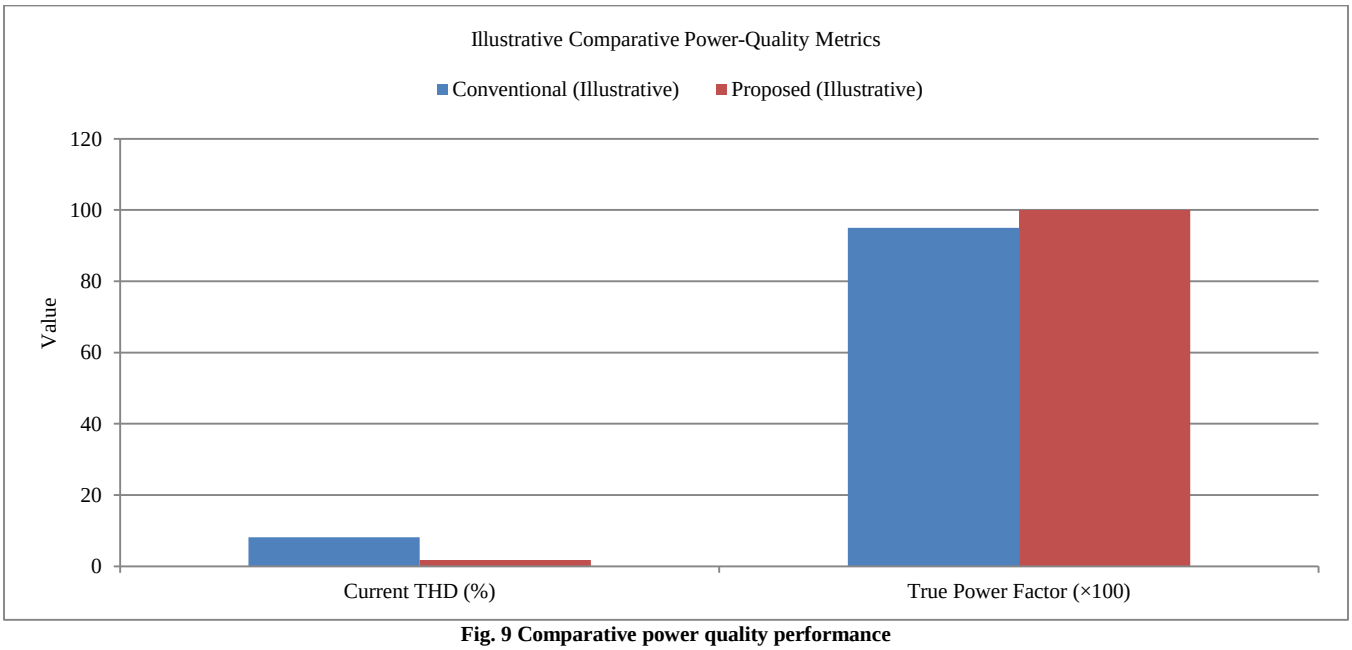

Fig. 9 Comparative power quality performance

Figure 8(a) shows the response of grid current, and Figure 8(b) shows the harmonic spectrum of grid current using the proposed STARC control strategy. The fundamental component prevails in the spectrum, and the harmonic components have significantly smaller amplitudes than the fundamental component.

It can be inferred that there is an effective suppression of harmonic components in grid current. The comparative performance of conventional and proposed controllers in terms of power quality is shown in Figure 9.

Conventional controller shows a grid current THD value of 8.5%, while the STARC controller shows a THD value of 2.1%; this corresponds to 75.29% improvement. In addition to this, the power factor is improved from 0.955 to 0.9993, which implies unity power factor.

4.4. Ablation Study: Role of Each Component

The ablation study analyzes the effect of every important component of the proposed STARC-controlled PV-battery EV charging system by considering each controller separately and observe how system performance is affected. Table 10 (Appendix) provides the ablation study where RHRAC, HST-CPIAC and their combination have been evaluated separately while maintaining the same operational parameters. Figure 10 illustrates the performance of the system after removing individual components from it.

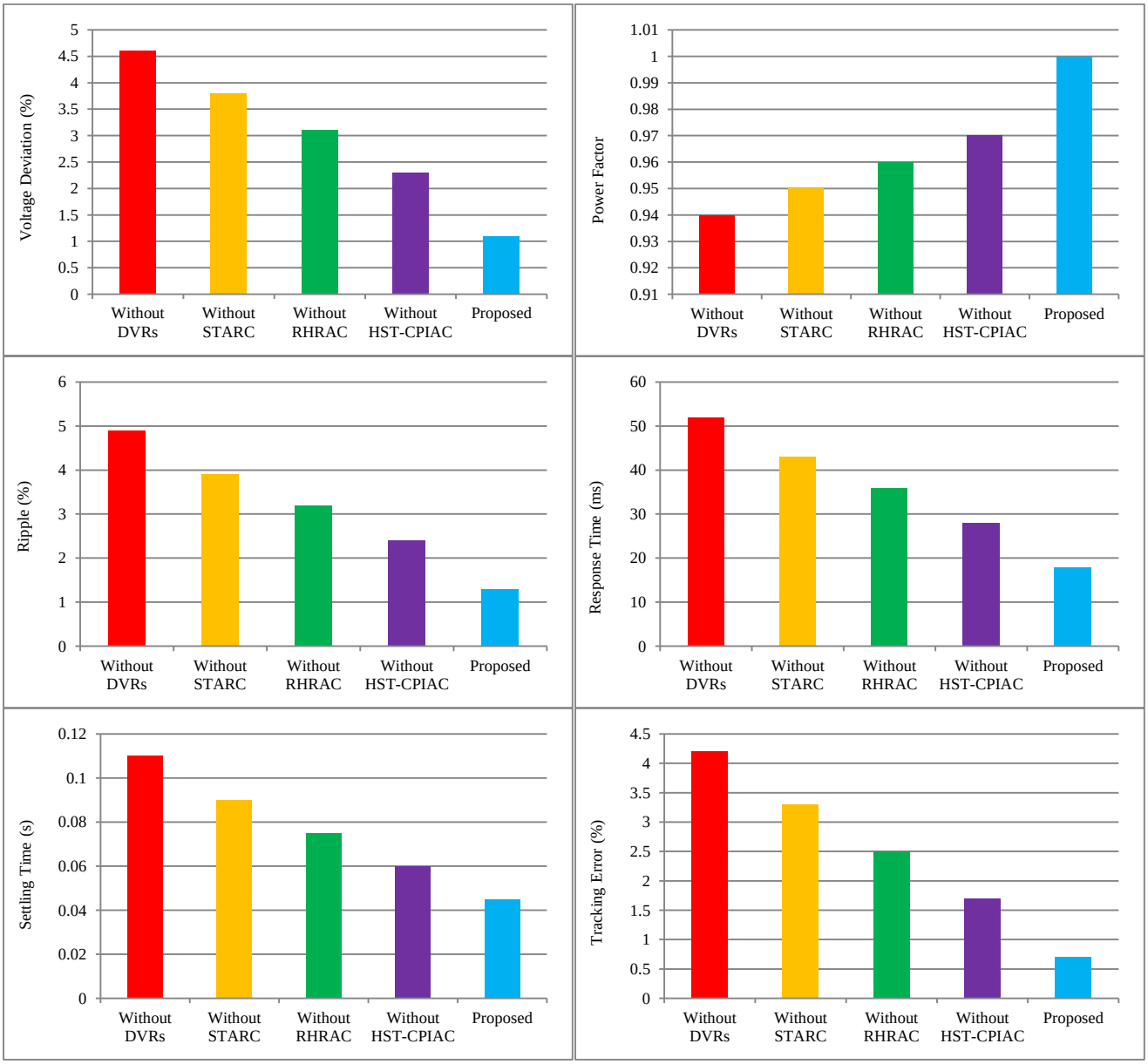

Fig. 10 Ablation study of the proposed framework

From Figure 10, when the system is designed without DVRs, it has the poorest performance, with a power factor of 0.94, voltage stabilization error of 4.6%, ripple of 4.9%, dynamic response of 52 ms, settling time of 0.11 s, and a tracking error of 4.2%. This again proves the importance of DVRs in stabilizing the grid against disturbances and ensuring

high voltage quality. However, the absence of STARC framework makes the system experience a fair improvement but with high ripple of 3.9% and slow dynamic response of 43 ms, thus suggesting the disadvantages of traditional control approaches. In addition, the absence of RHRAC causes poor grid-side control, as the power factor of 0.96 and tracking error of 2.5% are observed, thus stressing the importance of this approach for accurate current tracking and power factor correction. At the same time, the absence of HST-CPIAC brings about poor voltage regulation on the DC-link side, with the voltage ripple of 2.4% and the settling time of 0.06 s, thus demonstrating its significance for voltage fluctuation minimization. The full combination of DVRs with RHRAC and HST-CPIAC shows the best results, which can be presented as true power factor of 0.9993, voltage stabilization of 1.1%, ripple of 1.3%, dynamic response 18 ms, settling time of 0.045 s, and tracking error of 0.7%. These results confirm that the combined integration of DVRs, RHRAC, and HST-CPIAC ensures superior robustness, fast response, and enhanced power quality.

5. Discussion

The results of the simulation, as shown in Figures 5-7, validate the efficacy of the proposed STARC framework in providing improved dynamic and steady-state performance. The response of the EV current and DC-link voltage shows fast convergence with negligible overshoot and ripple. This ensures efficient energy transfer and charging. At the same time, the grid-side current has high sinusoidal purity and synchronization with the grid voltage, providing a high power factor with minimal harmonic content. In the case of the PV response, the results show effective MPPT operation.

From Table 7, the proposed STARC has a significant improvement compared to conventional control methods. Compared to the PI control method, the proposed STARC reduces the ripple from 5.2% to 1.3% and reduces the response time from 55 to 18 ms. In contrast, although the SMC method has better robustness, it still faces problems of chattering and has a higher ripple of 3.8%. This result is consistent with the finding in [15]. In addition, although the adaptive control methods can provide better steady-state accuracy, they have slower dynamics under disturbances, as also found in [12] and [13]. In the mSOGI control method, better synchronization and reduced distortion are obtained, but the dynamics and ripple performance are still not as good as the proposed STARC method. Recent studies, such as [18, 20], have shown the efficacy of super-twisting controllers in enhancing the stability of the DC-link, but they do not consider the adaptive control aspect for grid-side coordination. In addition, the hybrid control strategies proposed in [14] and [24] provide better stability, but they do not provide the desired performance during transients. The designed STARC scheme obtains better results through the combined operation of RHRAC and HST-CPIAC systems. The super twisting system ensures better transient control, and the use of adaptive gain tuning reduces the voltage oscillations and tracking errors under different conditions. The higher values of power factor can be attributed to the RHRAC, which is responsible for generating adaptive current references while keeping the quadrature axis current close to zero. Lower values of DC-link voltage ripple can be attributed to the HST-CPIAC, where the cascaded PI control takes care of eliminating steady-state errors and super-twisting control deals with fast rejection of any disturbance. Faster transient response is due to the quick response of the non-linear super-twisting controller and its adaptive gain control to large errors and sudden disturbances. As compared to traditional SMC, the new approach helps in reducing chattering through continuous super-twisting actions. As compared to adaptive and intelligent approaches, it does not depend upon any large training data set or complex computational process. The comparative results in Table 4 and the ablation study in Figure 9 support these explanations.

6. Conclusion

In this paper, a STARC control scheme is developed for a grid-connected PV-Battery EV charging system to achieve improved dynamic performance. This control scheme is based on integration of RHRAC control for grid-side current control and HST-CPIAC control for DC-link voltage control. Simulation results are obtained to validate the improved performance, achieving a power factor of 0.9993, improved ripple of 1.3%, fast response time of 18ms, and minimum tracking error of 0.7%. Comparative studies are conducted to validate the improved performance of the developed control scheme compared to existing control schemes. Based on the results obtained in this paper, a robust control scheme is developed, which can be used to achieve improved dynamic performance in next-generation EV charging applications under different operating conditions.

6.1. Limitations and Future Scope

Even though the proposed method has shown considerable performance improvement, the tuning of gains is nonlinear and complex, and the hybrid system also increases the computational complexity. In addition, there are several practical problems that can arise, such as measurement noise, time delays, and sensor inaccuracies, which can impact the performance of the system in practical scenarios. Therefore, it is recommended that the proposed system be implemented in real-time using a DSP/FPGA platform to assess the practical viability of the proposed system. In addition, the proposed system can be extended to multi-EV charging station systems and large-scale DC microgrid systems, which can increase the practical viability of the proposed system. In addition, communication time delays, cyber security, and fault-tolerant control can also be incorporated to increase the robustness of the system, and experimental evaluation under practical conditions and evaluation of the proposed system against other intelligent control methodologies can also increase the practical viability of the proposed system.

References

[1] Debalina De, Uttara Das, and Champa Nandi, "A Comprehensive Approach of Evolving Electric Vehicles (EVs) to Attribute "Green Self-Generation"-A Review," *Energy Harvesting and Systems*, vol. 11, no. 1, pp. 1-17, 2024. [CrossRef] [Google Scholar] [Publisher Link]

[2] Md. Naeem Hussain et al., "A Comprehensive Review of Renewable and Sustainable Energy Sources with Solar Photovoltaic Electricity Advancement in Bangladesh," *Control Systems and Optimization Letters*, vol. 2, no. 1, pp. 1-7, 2024. [CrossRef] [Google Scholar] [Publisher Link]

[3] Abhishek Kumar Tripathi et al., "Integration of Solar PV Panels in Electric Vehicle Charging Infrastructure: Benefits, Challenges, and Environmental Implications," *Energy Science and Engineering*, vol. 13, no. 4, pp. 2135-2152, 2025. [CrossRef] [Google Scholar] [Publisher Link]

[4] Darío Benavides et al., "Predictive Power Fluctuation Mitigation in Grid-Connected PV Systems with Rapid Response to EV Charging Stations," *Journal of Energy Storage*, vol. 86, pp. 1-20, 2024. [CrossRef] [Google Scholar] [Publisher Link]

[5] Ziad M. Ali et al., "Complexities of Power Quality and Harmonic-Induced Overheating in Modern Power Grids Studies: Challenges and Solutions," *IEEE Access*, vol. 12, pp. 151554-151597, 2024. [CrossRef] [Google Scholar] [Publisher Link]

[6] Shuiqing Xu et al., "Comprehensive Diagnosis Strategy for Power Switch, Grid-Side Current Sensor, DC-Link Voltage Sensor Faults in Single-Phase Three-Level Rectifiers," *IEEE Transactions on Circuits and Systems I: Regular Papers*, vol. 71, no. 7, pp. 3343-3356, 2024. [CrossRef] [Google Scholar] [Publisher Link]

[7] Gaurav Kumar Chaturvedi et al., "A Comprehensive Review on Dynamic Voltage Restorer Technologies: Architecture, Topologies, Control Strategies, and Deployment," *International Journal of Ambient Energy*, vol. 46, no. 1, 2025. [CrossRef] [Google Scholar] [Publisher Link]

[8] Nadir Abbas et al., "Survey of Advanced Nonlinear Control Strategies for UAVs: Integration of Sensors and Hybrid Techniques," *Sensors*, vol. 24, no. 11, pp. 1-51, 2024. [CrossRef] [Google Scholar] [Publisher Link]

[9] Bhabasis Mohapatra et al., "Optimizing Grid-Connected PV Systems with Novel Super-Twisting Sliding Mode Controllers for Real-Time Power Management," *Scientific Reports*, vol. 14, no. 1, pp. 1-21, 2024. [CrossRef] [Google Scholar] [Publisher Link]

[10] Vijaya Kumar Dunna et al., "Super-Twisting MPPT Control for Grid-Connected PV/Battery System using Higher Order Sliding Mode Observer," *Scientific Reports*, vol. 14, no. 1, pp. 1-17, 2024. [CrossRef] [Google Scholar] [Publisher Link]

[11] Aziz Watil, and Hamid Chojaa, "Enhancing Grid-Connected PV-EV Charging Station Performance through a Real-Time Dynamic Power Management using Model Predictive Control," *Results in Engineering*, vol. 24, pp. 1-16, 2024. [CrossRef] [Google Scholar] [Publisher Link]

[12] Aditya Sinha, Kenil Zalavadiya, and Kaibalya Prasad Panda, "Comprehensive Review of Adaptive Control in Solar PV Integrated EV Charging Station," *2024 IEEE Third International Conference on Power Electronics, Intelligent Control and Energy Systems*, Delhi, India, pp. 1084-1089, 2024. [CrossRef] [Google Scholar] [Publisher Link]

[13] Aqeel Ur Rahman et al., "Stability-Centric Design of a Droop-Mounted Adaptive Nonlinear Control for EV Charging in DC Microgrid," *IEEE Access*, vol. 12, pp. 123362-123375, 2024. [CrossRef] [Google Scholar] [Publisher Link]

[14] Manoj Kumar Senapati et al., "Advancing Electric Vehicle Charging Ecosystems with Intelligent Control of DC Microgrid Stability," *IEEE Transactions on Industry Applications*, vol. 60, no. 5, pp. 7264-7278, 2024. [CrossRef] [Google Scholar] [Publisher Link]

[15] Surabhi Bagherwal, and Subhasish Mahapatra, "Enhanced Stability and Control of Solar Powered EV Charging Stations using Disturbance Observer-based Adaptive Sliding Mode Control for DC Voltage Stabilization," *IEEE Access*, vol. 12, pp. 183293-183311, 2024. [CrossRef] [Google Scholar] [Publisher Link]

[16] Omar Zeb, and Iftikhar Ahmad, "Adaptive Barrier Synergetic Super-Twisting Control for Hybrid Energy Storage in Smart Electric Vehicle Charging Station with Recurrent Neural Network based MPPT," *SSRN*, pp. 1-18, 2025. [CrossRef] [Google Scholar] [Publisher Link]

[17] Suryakant Kumar et al., "Electric Vehicle Fast Charging Integrated with Hybrid Renewable Sources for V2G and G2V Operation," *IEEE Transactions on Industry Applications*, vol. 62, no. 1, pp. 165-178, 2026. [CrossRef] [Google Scholar] [Publisher Link]

[18] Ridha Benadli et al., "Robust Integral Super-Twisting Controller for Enhanced Photovoltaic Integration with Hybrid Battery and Supercapacitor Storage in DC Microgrid," *Results in Engineering*, vol. 24, pp. 1-22, 2024. [CrossRef] [Google Scholar] [Publisher Link]

[19] Rehanullah Wahidi et al., "Dynamic Control Strategies for Islanded DC Microgrids Integrating Renewable Energy, Fuel Cells, and Battery-EV Storage," *Franklin Open*, vol. 13, pp. 1-12, 2025. [CrossRef] [Google Scholar] [Publisher Link]

[20] S. Anbuchandran et al., "Dynamic Voltage Regulation in DC Microgrids using Super-Twisting Sliding Mode Controllers," *Electrical Engineering*, vol. 107, no. 11, pp. 14205-14227, 2025. [CrossRef] [Google Scholar] [Publisher Link]

[21] Krishnapada Mondal et al., "Super Twisting Sliding Mode Controllers based Grid Connected Hybrid Renewable Energy Sources Operated Power Supply System," *2025 International Conference on Computing Technologies*, Bengaluru, India, pp. 1-7, 2025. [CrossRef] [Google Scholar] [Publisher Link]

[22] Abdul Zeeshan, and Swapnil Srivastava, "Impact Analysis and Control of EV Charging on Grid Connected to Optimal Structure Hybrid Wind-Solar PV System," *International Journal of Engineering Systems Modelling and Simulation*, vol. 16, no. 6, pp. 335-353, 2025. [CrossRef] [Google Scholar] [Publisher Link]

[23] Monika Gupta et al., "Grid-Connected PV Inverter System Control Optimization using Grey Wolf Optimized PID Controller," *Scientific Reports*, vol. 15, no. 1, pp. 1-31, 2025. [CrossRef] [Google Scholar] [Publisher Link]

[24] Debasish Mishra, Bhim Singh, and Bijaya Ketan Panigrahi, "Multi-Source Energy Management in a Grid-Synchronized Bi-Directional EV Charging Architecture with Error-Modified Adaptive Control," *IEEE Transactions on Energy Conversion*, vol. 41, no. 1, pp. 213-224, 2026. [CrossRef] [Google Scholar] [Publisher Link]

[25] K.M. Sanjeeva Kumar et al., "Robust Control Strategy for PV-Battery Integrated UPQC in Electric Vehicle Charging Stations for Power Quality Enhancement," *2025 International Conference on Power Electronics and Energy*, Bhubaneswar, India, pp. 1-6, 2025. [CrossRef] [Google Scholar] [Publisher Link]

Appendix

Table 10. Ablation study

Component	Charging and discharging efficiency	Efficiency	Overall system efficiency	Dynamic response	Overshoot	Total Harmonic Distortion (THD)	Power oscillations	DC-link voltage deviation	Steady-state power oscillation	Voltage tracking error	State-of-Charge (SOC) tracking error	Convergence time	Settling time	Rise time
RHRAC	96.82	96.35	95.94	90.26	2.31	1.86	1.51	1.46	1.42	1.18	0.94	0.38	0.29	0.13
HST-CPIAC	97.21	96.84	96.42	93.18	1.82	1.57	1.12	1.17	1.05	0.94	0.68	0.31	0.24	0.11
RHRAC + HST-CPIAC (Proposed)	98.65	98.23	97.96	96.84	1.24	1.245	0.73	0.82	0.68	0.61	0.42	0.25	0.18	0.09